THE PREDICTION OF HEAT TRANSFER AND ABLATION IN THE AFT-CLOSURE OF A SOLID PROPELLANT ROCKET MOTOR

W. C. Kuby, Jr.
J. L. Richardson

Ford Motor Company
Aeronutronic Division
Research Laboratory
Newport Beach, California

ABSTRACT

A mathematical design model has been developed for the prediction of insulation requirements in the aft-closure of a solid propellant rocket motor. This model and the associated calculation technique represent only a first approximation to the exact solution of a problem concerned with various complex phenomena. The behavior of ablative elastomeric insulation materials in such an application is considered. The choice of the assumptions used to calculate the forced convective and radiative heat fluxes is based on recent experimental results. A summary is made of the information still to be determined in order that this model can be fully utilized.

The work described in this paper was performed under Air Force Contract No. AF 04(611)-7047, sponsored by the Air Force Flight Test Center, Air Force Systems Command, Edwards Air Force Base, California.

THE PREDICTION OF HEAT TRANSFER AND ABLATION IN THE AFT-CLOSURE OF A SOLID PROPELLANT ROCKET MOTOR

W. C. Kuby and J. L. Richardson
Ford Motor Company
Aeronutronic Division Research Laboratory
Newport Beach, California

INTRODUCTION

A continuing problem in the field of rocketry has been the protection of the rocket walls from the extreme temperatures and the high heat fluxes that exist. This problem has become more difficult in the case of solid propellant rocket motors since the introduction of metal powders to increase performance. The existence of the condensed-phase metal oxides in the combustion effluent has proved to create a severe environment, particularly in the aft-closure region. Despite the importance of understanding the phenomena that lead to this problem, no dependable method has been developed to predict the deleterious results of motor firings. The purpose of this paper is to delineate the problem and to indicate the areas in which more research work is necessary in order to understand the complex phenomena sufficiently to analytically predict the consequences in an unfilled (or filled) aft-closure region. In order to accomplish this end a calculation technique is outlined, and where suitable analyses exist, these analyses are discussed in detail. In those areas in which suitable analyses do not exist, the problem is defined and the necessary understanding indicated. Due to the complexity of the problem and the dearth of information in certain areas, many effects have not been considered. Among these effects are the complications of boundary layer reactions and their effect on heat transfer rates and surface regression rates, and the reduction of convective heat transfer caused by blowing.

DISCUSSION OF MODEL

The discussion presented herein will apply to an aft-closure configuration such as is shown schematically (see Figure 1). Although this axisymmetric case is possibly the simplest of configurations that one might choose, it merely serves as a starting point for such discussions of aft-closure problems. Theoretical analyses of subsonic jets of compressible fluids flowing into a compressible static fluid as discussed by Pai (1) show that the spreading angle of the jet is very small. These results have been verified by water model studies by Price, et al. (2), and they suggest that there are two separate flow regions in the aft-closure, one of which is a recirculation zone existing above the intersection of the boundary edge of the jet and the aft-closure wall; the second is the fast flowing fluid below this intersection. The significance of such a model is that there exist two distinct zones in which the factors controlling the ablation processes may be completely different. The first, the recirculation zone, is characterized by low convective heat transfer and

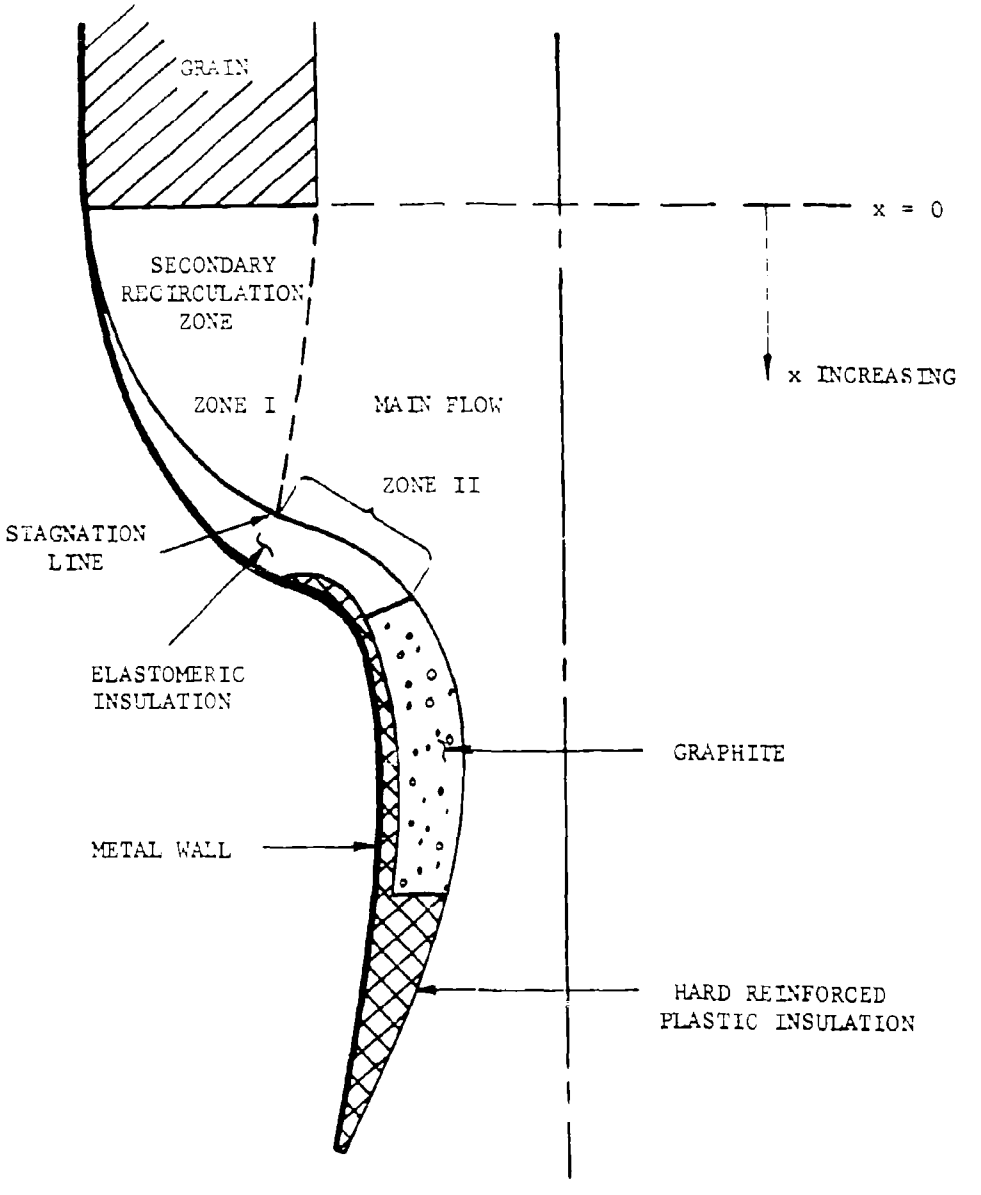

Fig. 1. Configuration at a Given Time

negligible particle effects. If the materials used in this zone form a char layer, the char layer growth is the controlling factor and the heat flux need not be determined. For non-charring materials the regression rate is dependent on the amount of heat flux to the surface. In the second region, the ablation rate is controlled by the amount of heat supplied to the surface and by the erosion of the particle stream. Another implication of this concept of two flow zones is that the particles contained in the outer regions of the jet must necessarily go through a severe turn in the general region of the aft-closure wall. This turn gives rise to high centrifugal forces which cause these particles to "slip" from the flow and impinge upon the aft-closure wall. The result of such impingement is an increase in the amount of heat transfer to the wall as well as an increase in the amount of mechanical erosion of the insulation materials. Finally, since the grain port hydraulic radius is a function of time, the extent of the two zones is a function of time. Consequently, the calculation technique should account for this time dependence. Also because of the movement of the separation point, the boundary layer, and thus the convective heat flux in Zone II, have time variations.

If use is made of the above-stated model having two flow regions in the aft-closure (see Figure 1), the problem necessarily separates into two approaches. In the recirculation zone for char-forming insulators, there exists a transient ablation process which is controlled by the char layer growth rather than the heat and/or erosion factors associated with the gas-particle stream. An analysis of this problem has been made by Grosh (3). The non-char case must be handled by empirical methods. In the second region the analysis to be used is based on the independent evaluation of the heat fluxes and the assumption that the total heat is the additive effect of each individual mode of heat transfer. Methods are discussed for calculating the convective heat flux as well as the radiative heat flux. Evaluating the heat flux associated with particle impingement as well as determining the mechanical erosion is found to be very difficult with the present state of the knowledge. In order to relate the heat fluxes and mechanical erosion to the aft-closure insulation material, a concept similar to the currently used Q* (see Eq. 38) is suggested. The main difference is that the parameter used in this paper is tailored to the requirements of the analysis discussed herein. Although the techniques put forth in this paper do not allow an accurate and complete determination of the consequences of the gas particle flow in a solid propellant motor aft-closure, they do indicate what knowledge is necessary to successfully attack the problem that exists.

ZONE I: THE SECONDARY FLOW REGION

Char Forming Materials - The Grosh Analysis*

In the secondary recirculation region it is assumed that there are very low surface-regression rates, and as a result the primary consideration is the transient transfer of heat through the insulation material with or without the formation of a surface char layer. The former case has been analyzed by R. J. Grosh (3), and Scala and Gilbert (4). Grosh's equations have been programmed for use in this region.

*The nomenclature for this section is defined as it occurs in the text.

The Grosh analysis is based on a simple extension of the well-known Neumann problem (5). For the case of a single phase change (i.e., virgin ablative material pyrolyzing to form a porous char and gaseous products), Grosh used the following one-dimensional equations to describe the transient temperature distribution in both the porous char layer and the virgin ablator (see Figure 2):

$$\frac{\partial T}{\partial t} - \nu\left(\frac{dX_1}{dt}\right)\left(\frac{\partial T}{\partial x}\right) = \alpha_1 \frac{\partial^2 T}{\partial x^2} \qquad 0 < x < X_1 \tag{1}$$

$$\frac{\partial T}{\partial t} = \alpha_s \frac{\partial^2 T}{\partial x^2} \qquad X_1 < x < \infty \tag{2}$$

where

T = temperature at any point (°F)
t = time (sec)
x = position measured relative to the stationary exposed outer edge of the char layer (ft)
α_1 = thermal diffusivity of the gas-porous char layer (ft^2/sec)
α_s = thermal diffusivity of the virgin ablative material (ft^2/sec)
X_1 = time-dependent position of the inside edge of the porous char layer (ft)
ν = parameter proportional to the difference in density of the gas in the porous char layer and the virgin ablative material (defined in Reference 3)(dimensionless)

and the initial and boundary conditions used are:

$$T = T_i \qquad x = x,\ t < 0 \tag{3}$$

$$X_1 = 0 \qquad t < 0 \tag{4}$$

$$T = T_o \qquad x = 0,\ t \geq 0 \tag{5}$$

$$T = T_1 \qquad x = X_1,\ t \geq 0 \tag{6}$$

$$T = T_i \qquad x = \infty,\ t = t \tag{7}$$

and

$$\left(\frac{\partial T}{\partial x}\right)_t \Bigg|_{x=X_1^-} = \gamma_1 \left(\frac{\partial T}{\partial x}\right)_t \Bigg|_{x=X_1^+} + \omega\left(\frac{dX_1}{dt}\right) \tag{8}$$

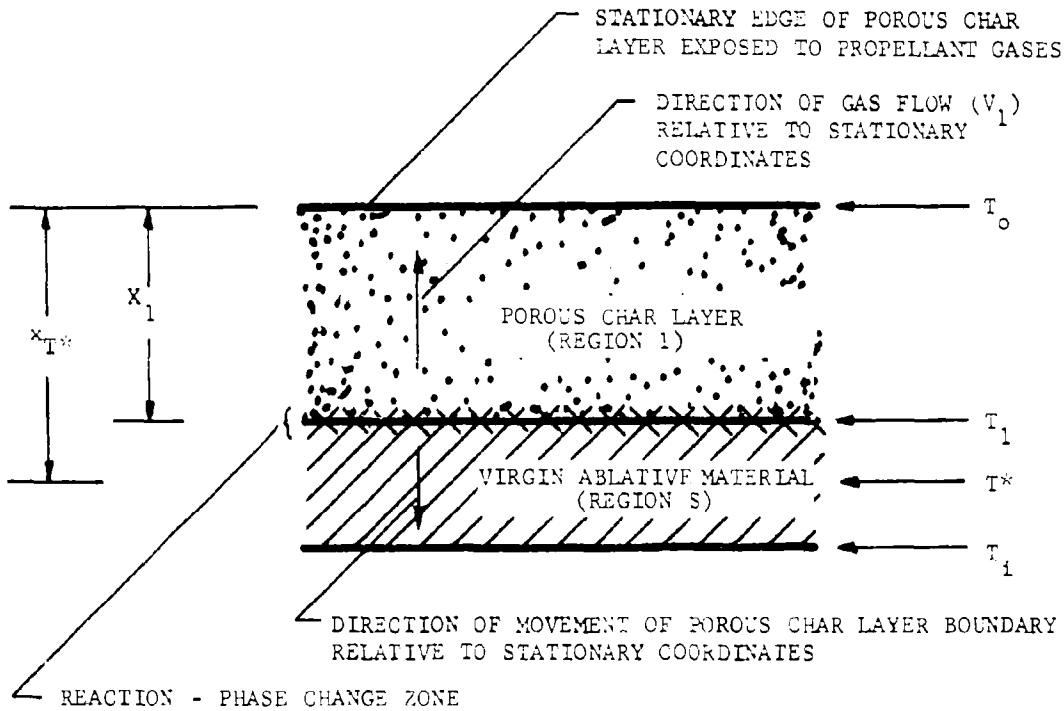

Fig. 2. One-Dimensional Char-Forming Ablator - Char Layer Not Removed (Symbols Apply to Grosh Analysis)

where γ_1 = the ratio of the thermal conductivity of the virgin material to that of the gas-char composite

and ω = quantity proportional to the sum of the heat of reaction (pyrolysis) and heat of sublimation (or heat of melting plus heat of vaporization) (sec °F/ft^2).

For this one-dimensional situation several important assumptions have been made in addition to those implied by Eqs. (3) through (8):

(a) The gas moves or transpires so slowly through the porous char that these two materials are in thermal equilibrium throughout the entire char layer.

(b) There is a step change in the physical properties of the char and virgin material at $x = X_1$, and the reaction zone thickness (i.e., presence) can be neglected.

(c) The physical properties of the materials are not temperature-dependent (average values employed).

(d) The composite (gas-char) thermal conductivity and mass-density/heat-capacity product can be adequately described by linear, porosity-additive expressions utilizing the properties of the pure materials.

The solution to the above equations is found in a manner similar to that utilized to obtain a solution to a modified Neumann problem (see Reference 5, p. 291, Eqs. (51) and (52)). The char depth is determined by the relation

$$X_1 = bt^{1/2}, \tag{9}$$

where b is the eigenvalue solution of a transcendental equation obtained from the moving-boundary condition (Eq.(8)) and is a function of the properties of the materials involved and the boundary temperatures assumed. For insulation materials which might be expected to conform to the Grosh model, it should be possible to measure b directly in the laboratory under the same conditions of surface temperature and pressure as would be encountered in the aft-closure which is being studied. The b so obtained could then be compared to that computed theoretically in order to arrive at better estimates for the char and virgin material properties.

The ablative materials for aft-closure applications which appear to be of greatest current interest are elastomers. Some form a char layer during ablation, while others form very little char, and that which does result has especially weak structural characteristics. Presently little is known about the properties of the char formed from elastomeric materials.

Using an elastomeric material and making estimates of the properties of the char produced by it, the computer program solution of the Grosh equations* is utilized to obtain the char thickness (X_1) and the heat penetration distance (x_{T*}) as a function of time. The x_{T*} is obtained from the following equation:

$$\left(\frac{T^* - T_i}{T_1 - T_i}\right) = \frac{\operatorname{erfc}\left\{\frac{x_{T*}}{2\sqrt{\alpha_s t}}\right\}}{\operatorname{erfc}\left\{\frac{b}{2\sqrt{\alpha_s}}\right\}} \tag{10}$$

(erfc denotes the complementary error function), where x_{T*} is the position at which the temperature is T* for a given time. The properties and boundary temperatures assumed for the example cases presented here are given (with their sources) in Table 1.

The results are presented in Figures 3 and 4. The calculations were performed for several different assumed values of the unknown properties of an elastomeric material. Cases 2, 3 and 4 utilized identical input information as employed in case 1 except for the one key property designated on the figures. For example, for case 3 the three relatively unknown properties which were assumed are the same as those used in case 1 except that L_1 = 200 Btu/lb is used in place of L_1 = 500 Btu/lb. The following is evident:

(1) The thermal conductivity of hydrogen is of greatest importance in determining the overall thermal conductivity of the transpiring gas phase, $k_{f,1}$ (for $x_{H_2} \geq 0.1$, say).

(2) The heat-penetration distance, x_{T*}, is only slightly greater than the char-layer depth, X_1, because of the much lower thermal conductivity of the virgin elastomeric material compared with that of the porous char (note that $k_{m,1}/k_s$ is on the order of 30 for $k_{m,1} \sim 1 \times 10^{-3}$ Btu/ft sec °F).

(3) For assumed values of gas composition and boundary temperatures, the results are most sensitive to the value assumed for $k_{m,1}$ (thermal conductivity of solid matrix material comprising the structure of the porous char). Considering the discussion given in Note 7, Table 1, concerning the range of thermal conductivity values which might be realistic estimates for the physical-thermal situation of interest here, and considering the fact that the thermal conductivity

*It should be noted that several typographical errors appeared in the original Grosh analysis (3). These were corrected before the equations were programed for the computer.

Table 1. Input to the Grosh Analysis

Properties and Boundary Temperatures	Explanations and Sources
1. T_o = 3000 F	1. Based on measurements of reference 39.
2. T_1 = 650 F	2. Estimate based on Aerojet material test data reference 7.
3. T_i = 100 F	3. Ambient conditions.
4. σ = 0.40, 0.65	4. Range of porosities typical of plastic chars (see reference 38).
5. (a) L_{1max} = 500 Btu/lb, (b) L_{1min} = 200 Btu/lb	5. Based on a rough extrapolation of Q* data to zero heat flux (reference 41) and estimates given for plastic ablators (see reference 38).
6. $k_{f,1} = 8 \times 10^{-5}$ Btu/ft sec °F	6. Based on assumed gas composition at 1 atm pressure and 1500°F; linear additivity combining rule used; data from reference 6, p. 461; pressure effect neglected; approximate extrapolation of data from 600 to 1500°F.
7. $k_{m,1}$ = (a) 1×10^{-3} Btu/ft sec °F, or (b) 8×10^{-3} Btu/ft sec °F	7. Data for non-porous petroleum coke at 200°F given on p. 457, reference 6. Data for σ = 0.40 porous graphite at 1500°F (see reference 42). Note that at 1000°F the thermal conductivity of this material is about 0.8×10^{-3} Btu/ft sec °F and that petroleum coke of 20-100 mesh has a thermal conductivity of 0.15×10^{-3} Btu/ft sec °F at 800°F, while powdered coke has a thermal conductivity of 0.031×10^{-3} Btu/ft sec °F at 200°F.
8. $k_s = 3.78 \times 10^{-5}$ Btu/ft sec °F	8. Thermal conductivity at 300°F, reference 41.
9. $\rho_{f,1}$ = 0.55 lb/ft^3	9. Computed from the perfect gas mixture law: $\rho_{f,1} = \frac{P_1 M}{RT_1}_{average}$, where $M = \sum_{i=1}^{4} x_i M_i$ (R = gas constant = 10.731 $\frac{ft^3\ psia}{lb\ mole\ °R}$; M_i = molecular weight of species i) with P_1 at 500 psia, T_1 at 1500°F. $_{average}$
10. $\rho_{m,1}$ = 94 lb/ft^3	10. Density of carbon stock (see reference 6, p. 457).
11. ρ_s = 80.5 lb/ft^3	11. Density at 300°F, reference 41.
12. $C_{f,1}$ = 0.42 Btu/lb °F	12. Frozen isobaric specific heat for assumed gas mixture composition $C \equiv C_p = \frac{\sum_{i=1}^{4} x_i \tilde{C}_{P_i}}{M}$, where $\tilde{C}_{P_i}$ = isobaric molar heat capacity of species i obtained from average values (60 to 3000°F) reported in reference 43 (M = 23 lb/lbmole).
13. $C_{m,1}$ = 0.387 Btu/lb °F	13. Specific heat for carbon. Average value for temperature range 130 to 2640°F (see reference 6, p. 235).
14. C_s = 0.48 Btu/lb °F	14. Heat capacity at 300°F, reference 41.
15. T* = 200°F	

Definitions of Terms

x_i = mole fraction of species i

σ = porosity of char

L_1 = heat of reaction + heat of phase change

k = thermal conductivity (Btu/ft sec °F)

ρ = mass density (lb/ft^3)

C = isobaric specific heat (Btu/lb °F)

Subscripts

1 denotes region 1, porous char-gas layer

s denotes region s, virgin material

f denotes gas evolved

m denotes solid matrix material of porous char

$$\left(\quad \right)_{f,s} \equiv \left(\quad \right)_s$$

Assumed Composition of Gas Given Off by the Ablating Elastomeric Material; $x_{H_2} = x_{H_2O} = x_{CO_2} = x_{CO} = 1/4$

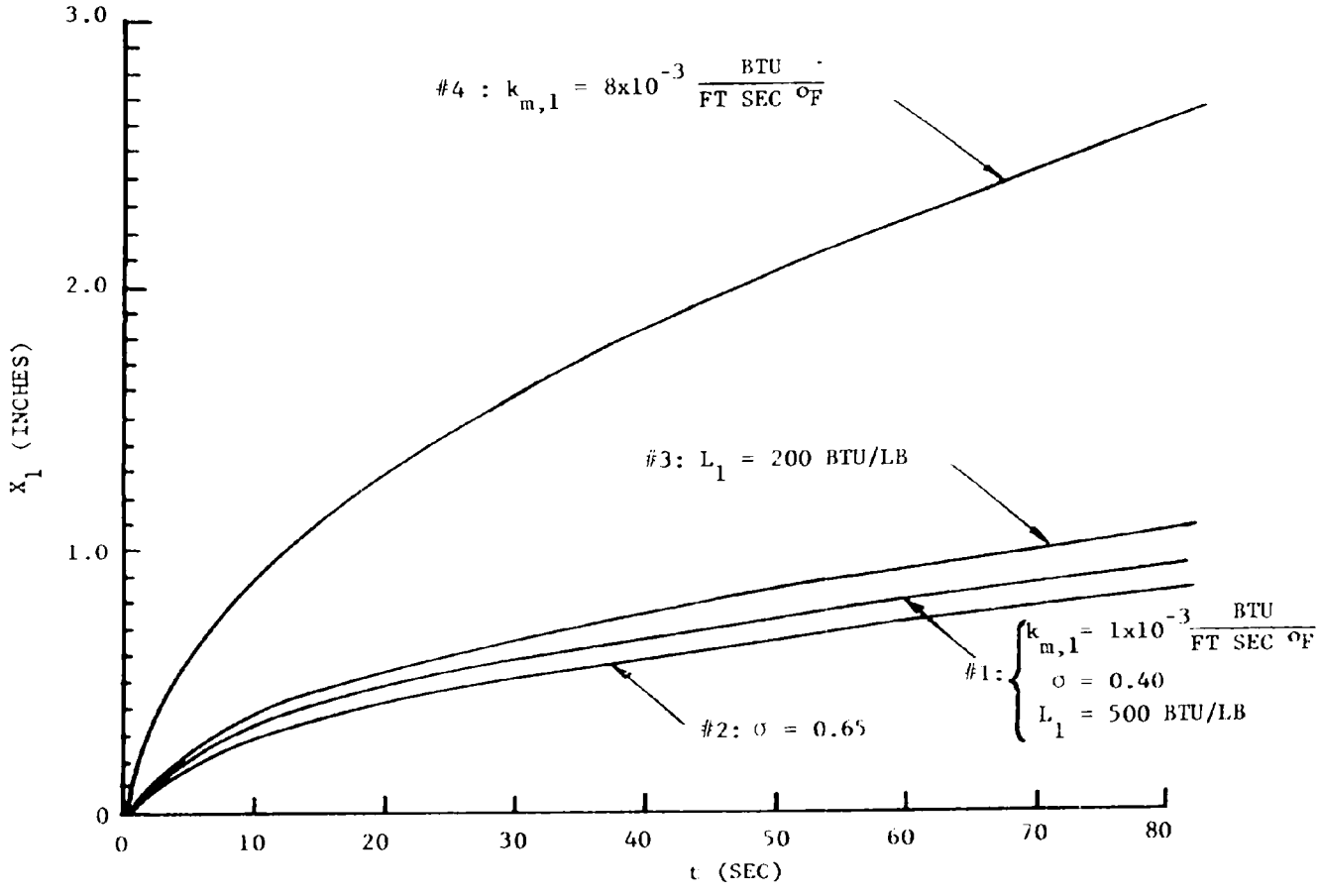

Fig. 3. Char Layer Thickness as a Function of Time

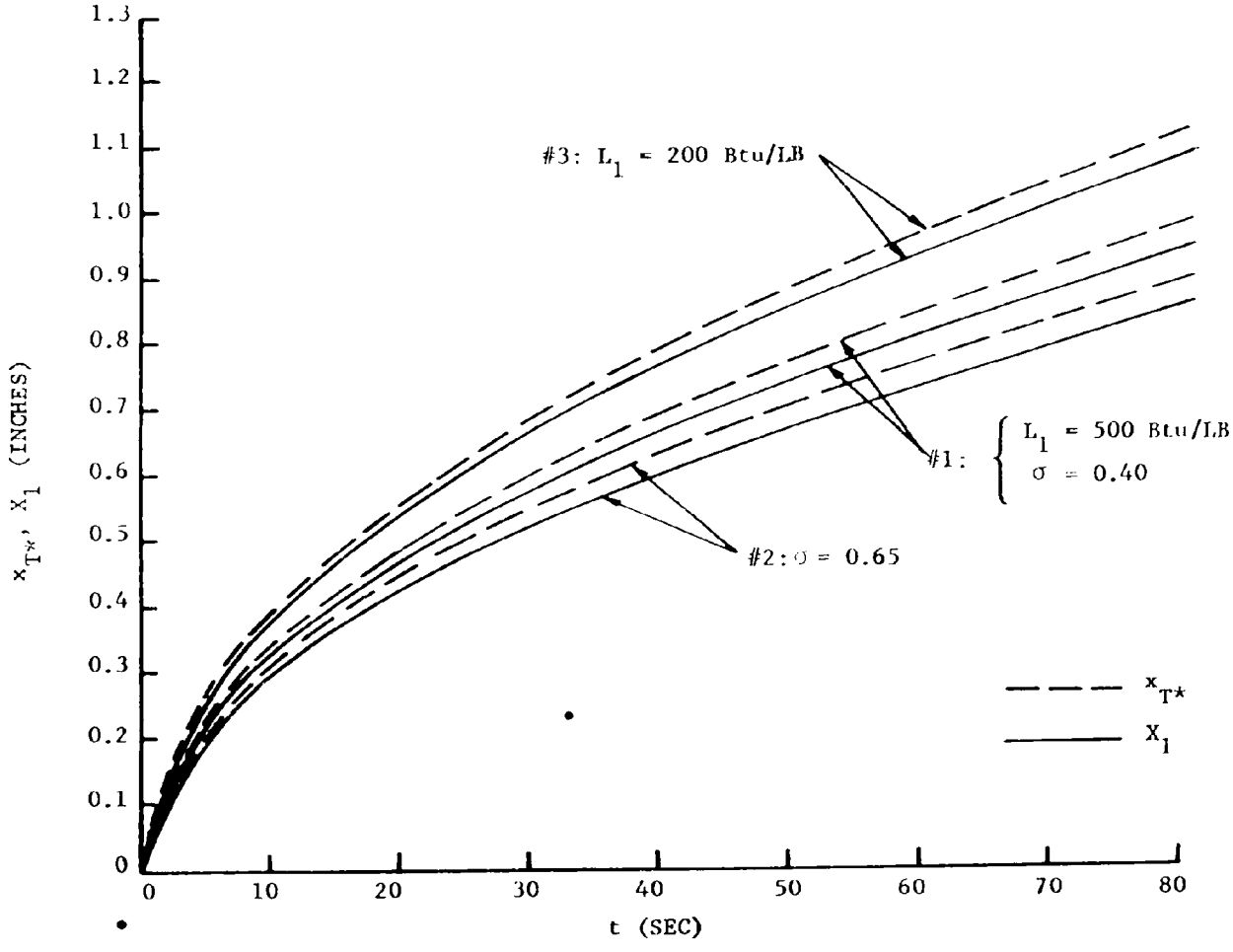

Fig. 4. Original Insulation Thickness Required to Keep Back Wall at 200°F and Char Layer Thickness as a Function of Time

of these materials in many cases decreases with increasing temperature, it is possible to assume that the $k_{m,1}$ should be somewhat less than 1×10^{-3} Btu/ft sec °F. (For example, the room temperature thermal conductivity of a porous carbon such as Carbocell grade 10 has $k_{m,1} \sim 0.5 \times 10^{-3}$ Btu/ft sec °F at room temperature (see Reference 6, p.1550).) This would yield char thicknesses on the order of tenths of an inch or less — a result which is compatible with char thicknesses actually obtained in hot test firings (7). The accuracy of the $k_{m,1}$ estimate will be the most important factor which will limit the usefulness of the Grosh analysis — or any other theoretical attempt to predict char-layer growth.

(4) The value assumed for L_1, the overall heat sink term (reaction plus phase change) has a modest influence on the results for the range of L_1 values which seem to be most appropriate for these elastomeric materials.

(5) For $0.4 < \sigma < 0.65$, porosity has little influence on the results.* This would not be expected to be true for extreme values of the porosity, i.e., for $\sigma \gg 0.65$ or $\sigma \ll 0.4$.

Nonchar-Forming Insulation Materials

If no char forms during the ablation process, the rate of material removal will be controlled by the heat flux to the surface. This heat flux is assumed to be the sum of convective and radiative fluxes. In a subsequent section of this paper a method is given for determining the convective flux in Zone II and the radiative flux in the aft-closure region. Since the velocities in the recirculation zone may be of the order of one-third those in the free stream (8), the convective heat transfer coefficient will also be about one-third the free stream value (see also Reference 9). Considering a gas-particle flow at 5500°R, a surface temperature of 3000°R, and a Zone II convective heat transfer coefficient of 0.5×10^{-3} Btu/in.^{2} °F sec, the convective flux is about 10% of the total flux. As a first approximation, therefore, one can consider only the radiative flux.

By using laboratory test data for Q*, the effective heat of ablation, the linear regression rate for the material is obtained from the following:

$$r \sim \frac{q_R}{\rho_{in.} Q^*} \tag{11}$$

*Recent laboratory measurements of the porosity of an elastomeric char indicated that σ (volume porosity measured at ambient conditions) at the top of the char layer which was exposed to the propellant gases was about 0.66, and at the reaction zone — char layer interface, was 0.75. The density of the solid matrix material, $\rho_{m,1}$, was about 103 lb/ft^3 (44).

This approximate value of the rate will be constant for any axial position in the aft-closure. An upper limit on the value of the regression rate is obtained by adding in a convective flux based on the forced convective transfer coefficient calculated for the first portion of Zone II.

ZONE II - THE HIGH HEAT FLUX REGION

In this region the controlling factor is the heat flux to the surface. This flux is assumed to be composed of linearly additive contributions from the mechanisms of forced convective, radiation, and particle impingement with energy accommodation at the surface.

Calculation of Convective Heat Transfer

Selection of Method. Analysis of aft-closure heating requires a method of predicting convective heat-transfer coefficients. Experimental results (10), (11) show that the convective heating in a rocket motor may vary by a factor of two or more, depending to a large extent on combustion variables. For this approximate analysis of aft-closure heat transfer, the effects of wall roughness, combustion instability, chemical reactions in the turbulent boundary layer and blowing have been neglected.* Each of the first three of these phenomena could be expected to increase the convective heat transfer rate to the surface, while the latter phenomenon would be expected to decrease the net heat flux to the wall.

The simplified Bartz (10) equation

$$h_c = \left\{ \frac{0.026}{D_*^{0.2}} \left(\frac{\mu^{0.2} C_p}{N_{Pr}^{0.6}} \right)_0 \left(\frac{P_c g}{C^*} \right)^{0.8} \left(\frac{D_*}{r_c} \right)^{0.1} \right\} \left(\frac{A_*}{A} \right)^{0.9} \sigma \qquad (12)$$

has been widely used for predicting heat transfer from rocket exhausts and is certainly accurate enough to do this within the scatter of the experimental data. Nevertheless, there is an important reason for using a more sophisticated method than the simplified Bartz equation for this analysis. One of the more important considerations in the aft-closure study is the prediction of the interaction between the aft-closure geometry and the heat transfer. Since the simplified Bartz equation is based on an empirical one-dimensional pipe flow equation assuming fully developed turbulent flow, it does not readily allow the inclusion of the effects of local variations in velocity and static pressure associated with the flow geometry. Instead, a method is required that will show these local time-varying effects of the nonuniform flow field in the aft-closure region upon the boundary layer and consequently the heat-transfer coefficient.

---

*Under conditions of chemical equilibrium in the propellant gas phase, the effects on the convective heat transfer due to chemical reactions can be appreciable in relation to the other effects which have been neglected (12), (13), and (14).

The Culick and Hill (15) application of the Truckenbrodt turbulent boundary-layer analysis (16) was selected. The Truckenbrodt analysis was chosen because of (a) its proved accuracy in incompressible boundary-layer analysis, (b) the ease with which time-dependent flow behavior can be accounted for, and (c) because, by using velocities at the edge of the boundary layer as input data (obtained from modeling, say, or a one-dimensional isentropic compressible flow calculation), it can include the effects of circumferential variations in the flow field in the estimation of the skin-friction coefficient. This analysis is recommended and discussed in detail by Schlichting*(see Reference 17, p. 580), and is valid for any arbitrary pressure gradient and velocity change at the edge of the boundary layer. It is based on the work of Rotta (17),(18), and depends on the stepwise integration of the energy integral equation along the surface. Culick and Hill have shown that, provided

$$H + 1 = (H_i + 1)\ (T_\infty/T) \qquad (13)$$

where H is the boundary-layer shape parameter (see Equation (15) of this report and Figure 22.7 of reference 17), it is possible to apply a Stewartson-Illingworth transformation to the y coordinate and convert the incompressible Truckenbrodt analysis to one valid for compressible flow. Culick and Hill have shown that for the case of little or no heat transfer, Equation (13) is valid for Mach numbers less than 5.

As an initial condition, this method requires a knowledge of the conditions of the laminar boundary layer just before transition to turbulent flow (ordinarily obtained from a laminar boundary-layer analysis). However, it should be sufficient for most aft-closure designs to assume a zero pressure gradient at transition and an arbitrarily thin momentum layer thickness, or to estimate the conditions at transition by considering a laminar flat-plate boundary layer using Michel's (19), (20) method to locate transition. It is not expected that the heat transfer coefficients calculated will be sensitive to the initial conditions, except very close to the transition point (see discussion relative to Figure 5).

Program Formulation. The Culick and Hill modification involves the use of several transformations to convert compressible flow input parameters into equivalent incompressible values. These equivalent incompressible flow quantities are used in the Truckenbrodt method which consists of the following steps: (1) the determination of the incompressible momentum thickness by an integration of a function of the velocity profile, (2) an integration involving the incompressible momentum thickness, δ_i, and a function of the velocity profile to determine the incompressible boundary layer shape factor L_i, and (3), the determination of the related shape factor H_i. Knowledge of δ_i and H_i as a function of axial position permits the calculation of the incompressible skin friction coefficient, C_{f_i}. The resultant C_{f_i}'s are converted to the equivalent compressible values of C_f. Finally, by using a modified Reynolds analogy (nearly identical in form to the Chilton-Colburn modification) the forced convective heat transfer coefficients are calculated from the values of C_f. Of course, in general the entire calculation must be repeated for several times during the firing in order to ascertain an adequate description of the time variation of h_c.

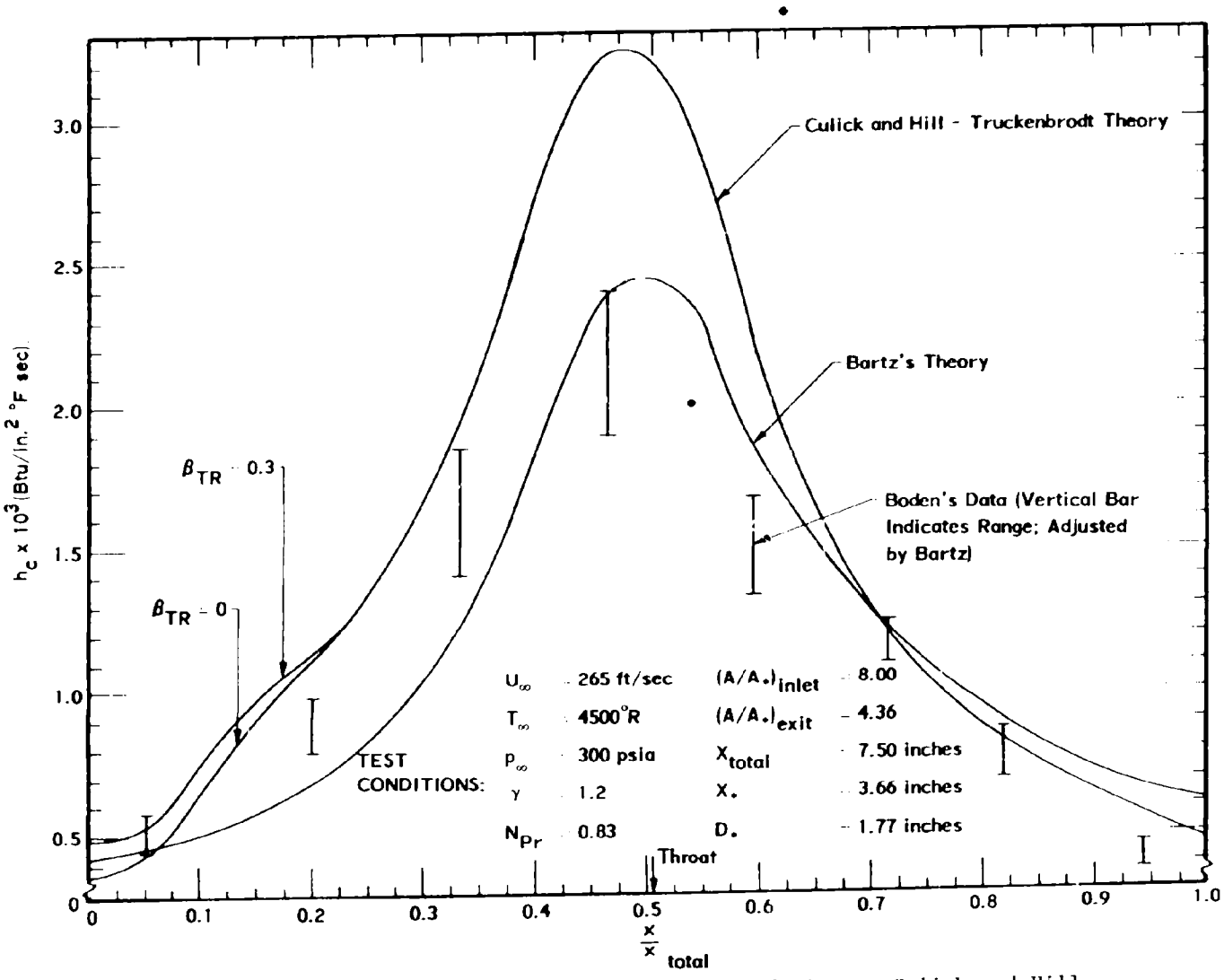

Fig. 5. The Forced Convective Heat Transfer Coefficient: Culick and Hill - Truckenbrodt theory, Bartz Theory and Experimental Results

The calculation is started by assuming (or calculating) the momentum thickness at the point of transition from laminar to turbulent flow, θ_{TR}, and the Falkner-Skan pressure gradient parameter at transition, β_{TR}. For most practical cases, θ_{TR} and β_{TR} can be assumed to be zero. Knowing the propellant gas velocity at the transition point, U_{TR},* and the kinematic viscosity of the propellant gas as a function of temperature and pressure, the momentum thickness Reynolds number at the transition point, $N_{Re_{\theta_{TR}}}$ may be calculated from

$$N_{Re_{\theta_{TR}}} \equiv \frac{U_{TR}\,\theta_{TR}}{\nu_{\infty}} \tag{14}$$

Tables of β_i versus $H_i\Big|_{Laminar}$, $N_{Re_{\theta_{TR}}}$ versus ΔH_i,

where
$$\Delta H_i \equiv H_i\Big|_{Laminar} - H_i\Big|_{Turbulent} \tag{15}$$

and $H_i\Big|_{Turbulent}$ versus $L_i\Big|_{Turbulent}$

are known and constitute part of the general input to the program. The absolute viscosity is estimated from Sutherland's law, which is

$$\mu = \mu_* \left(\frac{T}{T_*}\right)^{3/2} \left(\frac{T_* + 198.6}{T + 198.6}\right) \tag{16}$$

Sutherland's constant for air has been assumed to be applicable. The propellant gas density may be assumed, in a first approximation, to conform to the perfect gas law, thus,

$$\rho = \frac{PM}{R_o T} \tag{17}$$

The velocities, pressures, and temperatures at the edge of the compressible boundary layer are either measured in model experiments or computed as previously suggested. These values, along with the Prandtl number and the isentropic expansion coefficient of the propellant gas comprise the input quantities required to initiate the stepwise calculation from the transition point.

---

*The transition point is located near the stagnation point dividing Zones I and II, and thus the grain port velocity provides an estimate of U_{TR}.

The transformations of Culick and Hill, which are as follows:

$$U_i = \sqrt{\frac{T_\infty}{T}}\, U \tag{18}$$

$$\rho_i = \left(\frac{T}{T_\infty}\right)^3 \rho \tag{19}$$

$$x_i = \int \left(\frac{T}{T_\infty}\right)^{[(\gamma + 1)/2(\gamma - 1)] + 5/6} dx \tag{20}$$

and

$$C_f = C_{f_i} \left(\frac{T}{T_\infty}\right)^{5/6} \tag{21}$$

are applied to the input information to allow their subsequent use in the appropriate incompressible equations (see reference 17, equations 22.39, 22.32, and 22.31, as well as equation 42 of reference 16). The compressible skin friction coefficient, C_f, as a function of axial position and propellant burn-back time is thus obtained. Using the modified Reynolds analogy (21), (22),

$$h_c = \frac{\rho U C_p}{(N^*_{Pr})^{2/3}} \left(\frac{C_f}{2}\right) \tag{22}$$

where N^*_{Pr} is evaluated at the Eckert reference temperature, (12) defined by

$$T^* = \frac{T_w + T}{2} + (0.22)\, r' \frac{(\gamma - 1)}{2} M^2 T \tag{22a}$$

(r' is the recovery factor (see Eq. 25)),

and C_p is the isobaric specific heat, assumed to be a constant for the propellant gas system of interest and calculated from

$$C_p = \frac{\gamma R_o}{(\gamma - 1) Mg} \tag{23}$$

Comparison With the Bartz Equation. The solution obtained from Culick and Hill's modification of the Truckenbrodt analysis was programmed. Using this computer program, a sample calculation was made for comparison with the rocket motor heat-transfer data reported in references (10) and (11). It should be observed, at least for the data of these references that (a) Bartz's method tends to slightly over-predict the heat transfer in the exit portion of the nozzle, (b) the experimental results showed a maximum deviation of 80 percent above and 45 percent below the analytical values at the throat, and (c) the experimental results were found to be as much as 100 percent

above the analytical values in the entrance to the nozzle (note Ziebland's prediction (23) of the importance of entrance effects in this region).

Figure 5 presents experimental results for a test performed using the same rocket motor as was used by Welsh and Witte. These data were used as a comparison between results from the Culick and Hill - Truckenbrodt analysis and the Bartz analysis (24). Both sets of analytical results, together with the experimental results, are shown. It can be seen that the heat-transfer coefficient calculated by the present analysis agrees well with the experimental data in the exit portion where the coefficient based on Bartz's method is slightly high. At the throat, the present method gives results about 30 percent above both Bartz's results and the experimental data, and it predicts values higher than the Bartz equation in most of the entrance region, although farther upstream there is a crossover in the results (for $\beta_{TR} \equiv 0$). The set of experimental results in Figure 5 lie between the two analytical predictions. The data of Welsh and Witte for the entrance and throat region are often above the Bartz equation result and tend to be nearer the value predicted by the present method. Although there is considerable scatter in the experimental data, it can be seen that the present analysis compares well in all sections of the aft closure, throat and exit cone.

The importance of the assumed or calculated transition quantity, β_{TR}, on the computed forced convective heat transfer coefficient, h_c, is also shown in Figure 5. For a large variation in values of β_{TR}, the importance of this parameter rapidly diminishes with distance through the aft-closure, and has a negligible influence on h_c beyond about one-half of the way through the aft-closure entrance section of the nozzle system for which the curves and data in Figure 5 were obtained. Similar results were obtained when the δ_{TR} was varied by an order of magnitude (0.001 ft to 0.0001 ft).

Using the coefficient determined by the method of Culick and Hill, the convective heat flux can be obtained by the equation

$$q_c = h_c \left[T_{aw} - T_w \right] \tag{24}$$

providing a reasonable estimate of T_w can be made. The adiabatic wall temperature (or recovery temperature) can be calculated from

$$r' = \frac{T_{aw} - T}{T_o - T} \tag{25}$$

where $r' = N_{Pr}^{1/3}$ for turbulent flow over flat plates (25), (21). For rocket effluent gases r' is approximately 0.9 (i.e., $N_{Pr} \approx 0.7$), and therefore, since the Mach number is low (i.e., $T_o \approx T$) in the aft-closure region,

$$T_{aw} \approx T_o \tag{26}$$

or

$$q_c = h_c \left[T_o - T_w \right] \tag{27}$$

Particle Effects

The existence of alumina particles in the exhaust gases of a solid propellant rocket create a severe environment for the materials which are used to inclose the aft end of the rocket. Ungar (26) has demonstrated that if such gas-particle flows impinge on ablative surfaces, the rate of material removal is increased over that for a similar gas flow. The primary reasons for this severe condition leading to the increased material loss are the larger heat transfer rates caused by the paricles and the mechanical erosion of the surface due to particle-surface interaction. The increase in heat transfer is a threefold effect: first, the particles interact with the boundary layer, thus increasing the convective heat transfer; second, the particles penetrate through the boundary layer and transfer a portion of their kinetic and thermal energy to the wall upon collision; and third, the presence of a particle cloud effect increases the radiant heat flux to the surface. The significance of the mechanical erosion is believed to be the removal of the thermal insulating char layer which most materials form and the subsequent removal of virgin material through mechanical erosion.

The first two heat transfer effects are very difficult to evaluate on the basis of current knowledge. As a result their total effect will be lumped together and consideration will be given to the additive result. The method proposed is to use proportionality factors analogous to the accommodation factors defined in free molecular flow in order to prescribe that amount of energy which the particles contain that is transferred to the wall during collisions. Thus one can write the heat flux due to particle impingement as

$$q_p = \dot{m}_p \left[\alpha_t c (T_p - T_w) + \alpha_k \frac{U^2}{2 g_c J} \right] \tag{28}$$

where α_t and α_k are these proportionality factors. Since the particle velocities are relatively small in the aft-closure and the particle enthalpies are large, the total kinetic energy which the particles have is small in comparison with the thermal energy. Thus one can simplify by allowing α_k to equal 0 and considering only the thermal accommodation coefficient. It has been shown by Farbar and Morley (27) that the heat transfer rate is not increased appreciably at particle to gas loadings of ϕ less than 1.0 for straight pipe flow. Since the particle loadings in most rocket motors are considerably less than $\phi = 1.0$, it can be assumed that the heat transfer due to particle impingements will only be significant in those regions where the flow must go through large turning angles as discussed previously. Consequently simulated flows with particles are necessary to delineate these areas. Ungar (26) has analytically examined results obtained using materials that form liquid layers and successfully correlated his results. However, these results are not general enough to extend to other systems and will not be discussed further. Since very little information is available as to the values of the thermal and kinetic accommodation coefficients, the true importance of this heat flux cannot be evaluated. However, it is apparent that it may be sizable at positions of large turns and may be the factor which accounts for the high erosion rates in small sections of the aft-closure.

The presence of a large number of alumina particles in the solid rocket exhaust gases increases the importance of heat transfer by radiation. Investigators of heat transfer in liquid propellant rocket nozzles have assumed that the heat transfer by radiation from the exhaust gases was negligible. This assumption is based on the fact that the hot gases do not radiate an energy continuum but radiate only in small finite frequency bands. Although in these bands the radiation may be of black body intensity, the total radiancy from the gas is much less than the black body value. The presence of a solid phase which is emitting a continuum increases the overall radiation level. If this cloud is sufficiently dense, the effective emissivity can approach unity. Recently some experimental work has been carried on by Carlson (28) to measure the radiance of particle clouds in the exhaust of solid rockets. Further, a method (29) has been reported to quantitatively calculate on the basis of theory the emissivity of particle clouds. Both the experimental results and the theoretical method will be discussed with particular emphasis on their applicability to alumina clouds as found in rocket exhausts.

The experimental results reported by Carlson (28) are for the radiation from MgO clouds in an RP-1/gaseous oxygen flame. A slurry of RP-1 and MgO particles was combusted with gaseous oxygen in a rocket motor and the effluent expanded through a nozzle. The radiation of the cloud was measured at an expansion ratio of 5.0. The throat diameter was 1.25 inches. In the tests both the fuel-to-oxidizer ratio (the flame temperature) and the weight of particles-to-weight of gaseous effluent were varied. The results are shown in Figure 6. Since the optical properties are relatively insensitive to particle temperatures, the absorptivity is not expected to be highly dependent upon the oxygen-to-fuel ratio, and the data points of Figure 6, therefore, include several values of the oxygen-to-fuel parameter. The size distribution of the MgO particles is given in Figure 7.

The results shown in Figure 6 are correlated by the expression

$$\epsilon = 1 - e^{-k\zeta} \tag{29}$$

the form of which can be arrived at from theory. It has been shown (30) that the absorptivity of a particle cloud is given by the following relationship

$$\alpha = 1 - \exp\left[X \int_0^\infty \pi R_p^2 N(R_p)\, Q_{ext}(R_p)\, dR_p \right] \tag{30}$$

where

$$Q_{ext}(R_p) = \frac{\sigma_{abs} + \sigma_{sc}}{\pi R_p^2} = \frac{\sigma_{eff}}{\pi R_p^2} \tag{31}$$

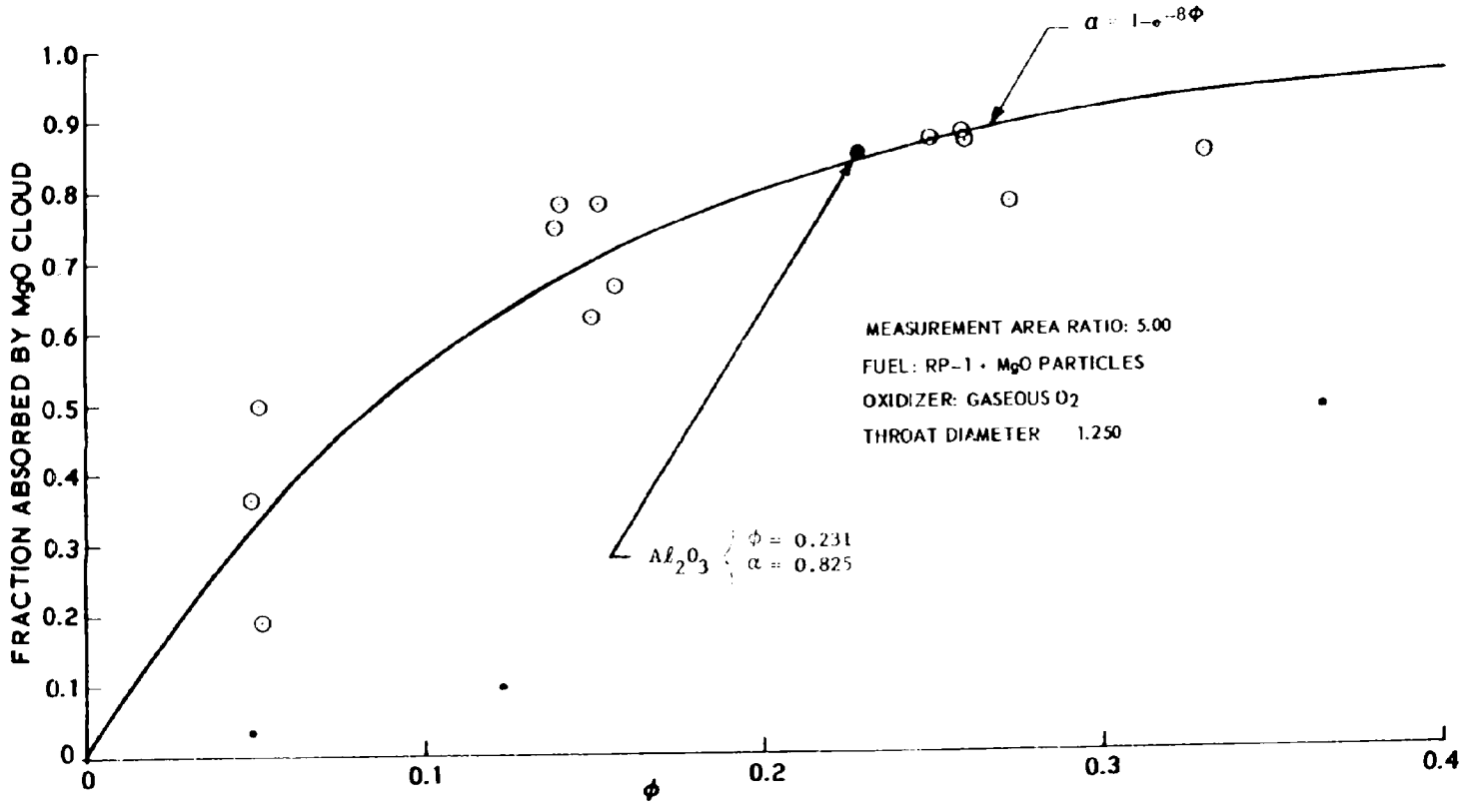

Fig. 6. Absorptivity of Rocket Exhaust Due to Presence of MgO Cloud - Wavelength of Measurement = 5911 Angstroms

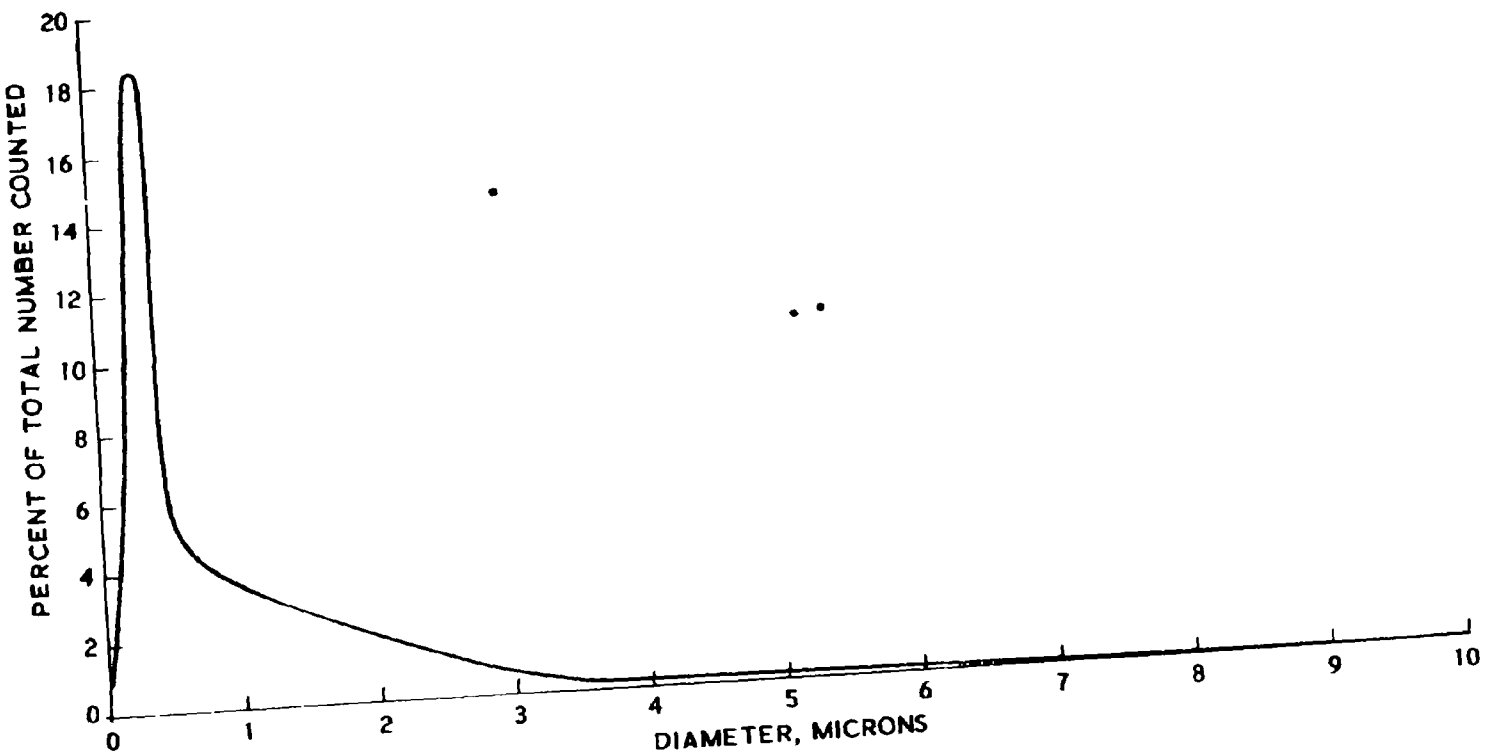

Fig. 7. Distribution of MgO Particle Sizes Used in Velocity-Lag Tests

Assuming that all the particles in the cloud are of the same radius this expression can be integrated to yield

$$\alpha = 1 - \exp(NX\sigma_{eff}) \tag{32}$$

Also

$$\phi = \frac{N(\frac{4}{3}\pi R_p^3)\ \rho_{particle}}{\rho_{gas}} \tag{33}$$

where ϕ is the ratio of the mass flow rates of particles to gas. Substituting for N in Eq. (32) gives

$$\alpha = 1 - \exp\left[\left(\frac{6}{\pi D^3 \rho_s}\right)\rho_g\ X\phi\sigma_{eff}\right] \tag{34}$$

If exhaust clouds contain the same chemical species of particles (i.e., same optical properties), having the same size distribution, and if radiancy measurements are made at the same area ratio, Eq. (34) can be reduced to the expression used to correlate the results of Figure 6.

If these same conditions apply to two different motors, the following ratio is obtained from Eq. (34):

$$\frac{\ln(1 - \alpha_1)}{\ln(1 - \alpha_2)} = \left(\frac{\rho_{g_1}}{\rho_{g_2}}\right)\left(\frac{X_1}{X_2}\right)\left(\frac{\phi_1}{\phi_2}\right) = \eta \tag{35}$$

or

$$\alpha_1 = 1 - (1 - \alpha_2)^{\eta} \tag{36}$$

Eq. (36) allows the estimation of the emissivity of a given cloud based on an experimentally determined emissivity of another cloud. In order to extend the applicability of the MgO data, Carlson has also fired the slurry motor using alumina rather than MgO particles. The results of these tests have not been reported to date; however, one point which has been measured is included in Figure 6. Although the amount of data is quite small, the good agreement between the alumina emission and MgO emission lends some support to the use of this data to approximate the emissivity. By using the results of this one test and Eq. (36), the following relationship is obtained:

$$\alpha = 1 - 0.175^{\eta} \tag{37}$$

If one now can consider a motor having a 20% aluminum loading; that is, a ϕ of 0.67, it is seen from Eq. (37) that an emissivity of 0.99 will be obtained for a diameter of about 2.7 inches. Although the results of this calculation

do not allow one to accurately determine the emissivity of a particle cloud at any position for any motor, it is felt that it does show that the effective emissivity of the particle clouds in motors of the size of current interest is close to unity.

A method of calculating the radiancy of particle clouds has been carried out by Stull and Plass (29). The particular problem solved by them was for solid carbon particles in flames; however, the method is applicable to the solid propellant case if one knows the optical properties of the alumina at the elevated temperatures encountered. The method that is outlined by Stull and Plass allows the determination of the scattering and absorption cross-sections for the individual particles as calculated from the Mie theory. A dispersion equation is derived which represents the optical properties of the carbon at the elevated temperatures. Based on these values an expression is obtained for the radiation intensity emitted by a large number of dispersed particles which includes all higher order scattering processes. Stull and Plass demonstrate this technique for particle clouds containing single sized particles (Distribution I) and for two different size distributions as shown in Figure 8 (Distributions II and III). Figure 9 shows typical results obtained in this study where λ is the optical cross section of the cloud. As one might expect, at higher optical cross sections, the radiation intensity or emissivity approaches black body conditions. It should also be pointed out that this method is limited to particle distributions in which all the particles are at the same temperature. It has been shown that, as the particles are accelerated in the nozzle, a velocity and temperature lag develops which is a function of the diameter of the particles (31). As a result not only is there a particle size distribution in the nozzle but there also is a particle temperature distribution which is a function of the size distribution. Before the method of Stull and Plass can be applied throughout the nozzle, the derivation must be revised to include this temperature variation.

The principle reason that this theoretical approach is not utilized at present is the lack of data as to the optical properties of alumina at temperatures that are typical of those found in rocket exhausts. There are several programs under consideration that will lead to a better understanding of the overall problem including the evaluation of the optical properties of alumina in exhausts. However, until this work is completed only empirical predictions of the cloud emissivity based on an insufficient quantity of data are available. Another problem in the use of the empirical data is that the maximum intensity for the radiation occurs at smaller wave lengths than the corresponding black body intensity maximum (see reference 29). As a result, the concept of an effective emissivity is not valid; that is, the cloud does not act as a "gray" body. Although this is not a serious error for clouds whose emissivity is near unity, it could introduce error at lower emissivities. Also Stull and Plass show that the emissivity of a cloud of size distributed particles is not the same as that for a cloud of the same number of particles, all having the diameter that is the mean of the distributed cloud. Carlson (28) pointed out that the radiation from a cloud having a temperature distribution as discussed previously radiates like a single sized cloud of particles whose diameter and corresponding temperature was greater than the distributed cloud mean. In short, the radiation from clouds of particles having a size

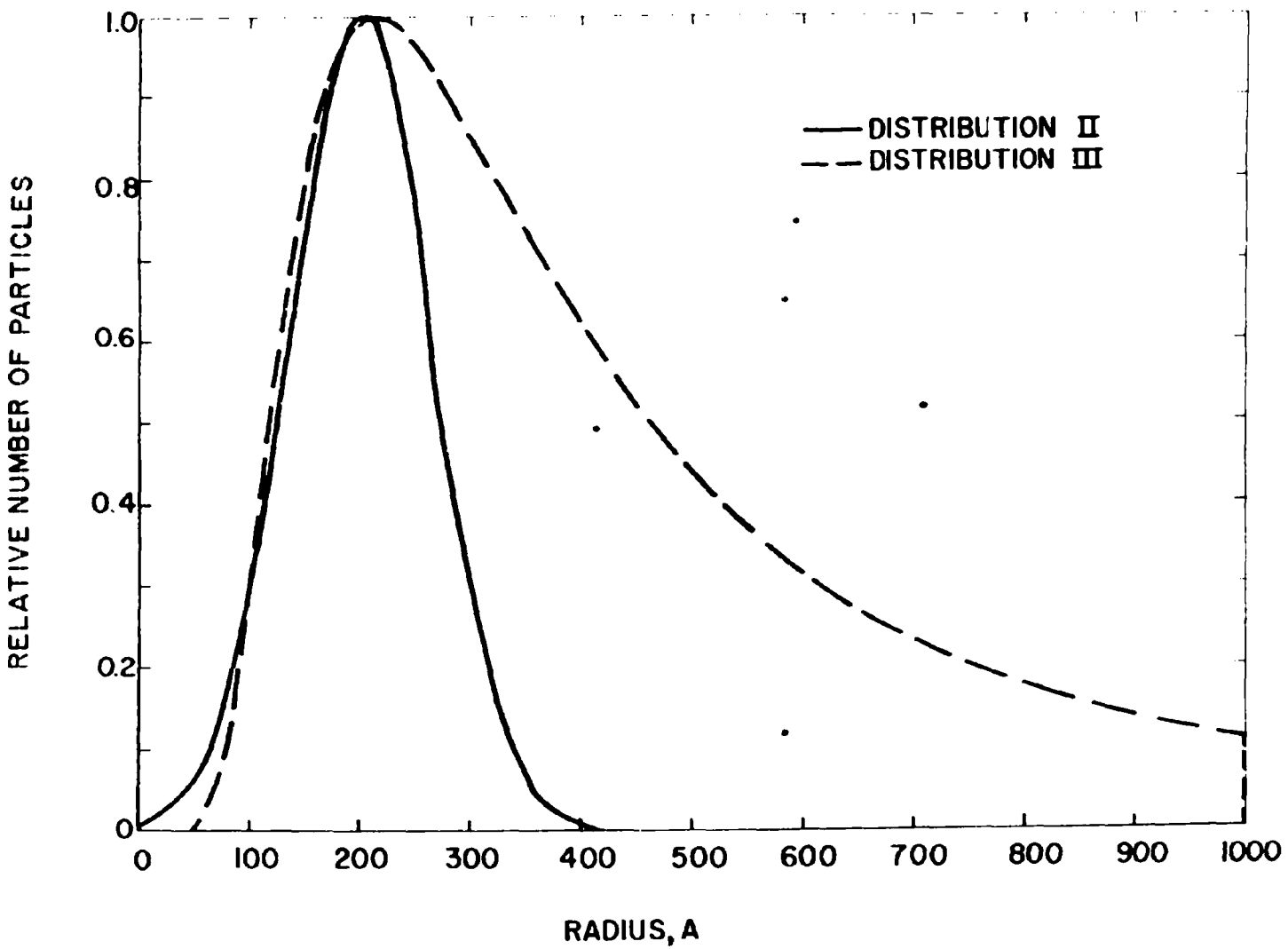

Fig. 8. Two Particle Size Distributions Used for the Calculation of the Emissivity of Carbon Particles

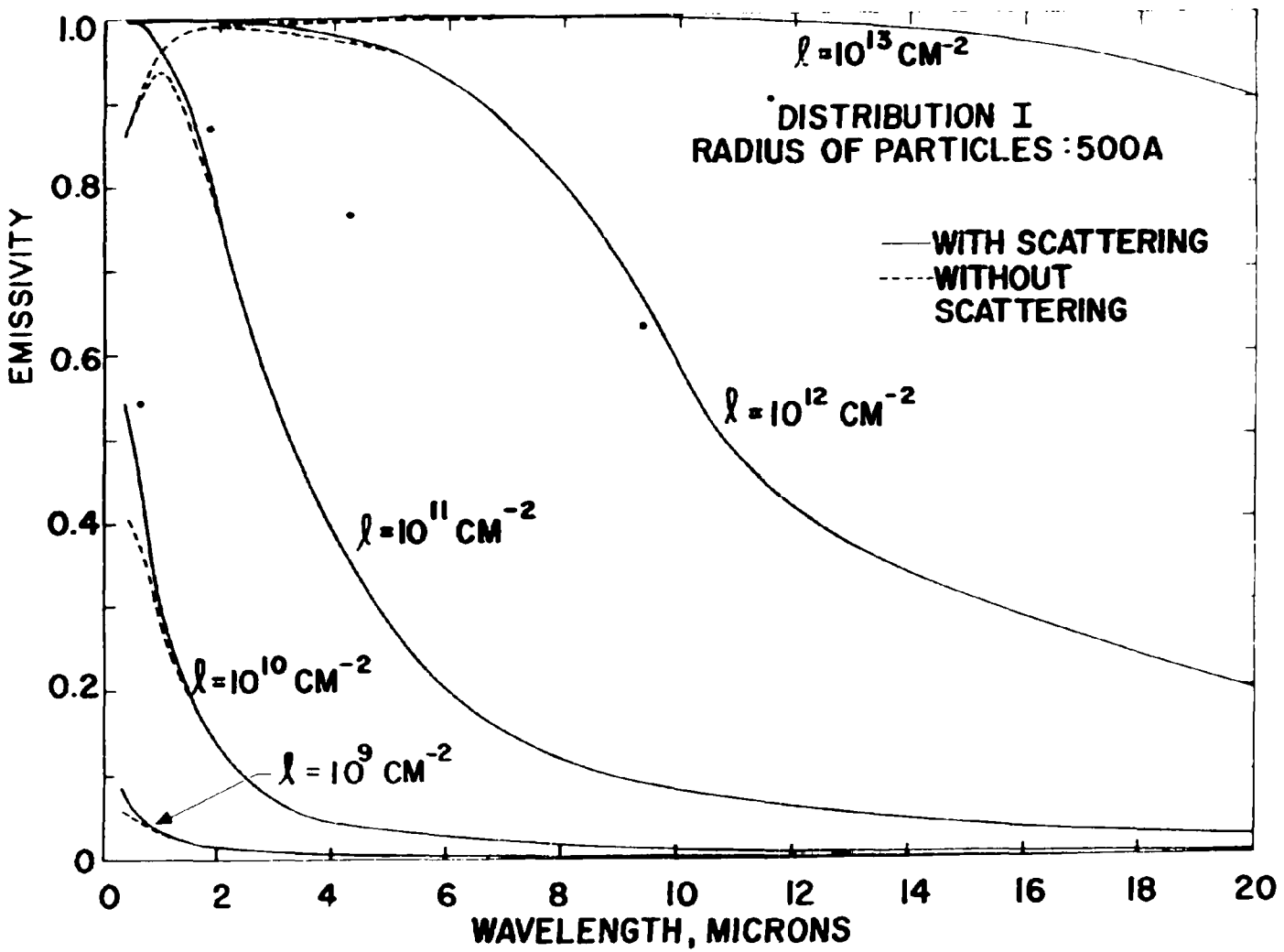

Fig. 9. Emissivity as a Function of Wavelength for Carbon Particles of 500 A Radius

distribution does not bear a simple relation to the radiation from a similar single sized cloud of particles of the distribution mean diameter.

In the aft-closure region of most current motors many of these limitations have only a minimal effect on the radiative heat flux, but they are reported as a warning against an indiscriminate application elsewhere. Considering only the aft-closure region of highly loaded metallized solid propellant motors of large diameters (typical diameters are greater than six inches), it has already been shown that the cloud emissivity is near unity and the particles are all in equilibrium with the gas at the gas stagnation temperature. Consequently, the radiant flux can be written as

$$q_r = \epsilon\sigma\left[T_o^4 - T_w^4\right] \tag{38}$$

where

$$\epsilon = \left(\epsilon_{wall}^{-1} + \epsilon_{cloud}^{-1} - 1\right)^{-1} . \tag{39}$$

The most important effect of particle impingement on the wall is that of mechanical erosion. As discussed previously this mechanical erosion may well remove the thermal insulating char layer that most aft-closure insulation materials form during firing. Once this insulating layer has been removed, the heat transfer to the virgin material is increased, thus increasing the ablation rates. Also, the particles can then mechanically erode the virgin material. The significance of this model is that it is not necessary to consider the ablation in evaluating the mechanical erosion, so that cold flow tests with particles impinging upon cold surfaces will give an estimate of the erosiveness of the stream. By relating the amount of particle impingement at a particular point to these cold flow tests, one can acquire a reasonable estimate of the virgin material removal due to erosion. Moreover, a simplified model based on no char layer ablation can be analyzed in order to estimate the amount of virgin material removal due to thermal degradation of the insulating materials. Again the validity of such a model is in question, but by pointing out the possibility of the existence of such a model it is hoped that emphasis will be placed in future experimental work upon the evaluation of these particle effects.

Ablation Rate Determination

In Zone II the insulation material ablation rates are large and will be strongly influenced by particle effects. The variation with time of the hydraulic radius of the grain port and the grain port design itself are important factors which cause the fluid flow in Zone II to be three dimensional and unsteady. It is apparent that when this complexity is coupled with that of two-phase flow and ablation, no analytical methods are available for the prediction of the heat and mass transfer rates at the wall. The approach used here is to employ an effective heat of ablation, Q*, which is in part a material property, in order to estimate the insulation material removal rate. The Q* concept has been extensively discussed in the literature of ablation (32), (33), (34), (35), (36), (37), (4). The effective heat of ablation is defined by (35),

$$Q^* = \frac{\text{heat transfer to a non-ablating calorimeter}}{\text{total mass ablated}} \tag{40}$$

where the calorimeter is assumed to have the same surface temperature, emissivity, and catalytic efficiency as the ablating material. If, in a laboratory determination of Q* for an ablating material which forms a char layer (which may or may not be structurally weak), care is taken to retain all the solid material (virgin elastomer plus char particles and layer) by containing the sample in a short length of a cylinder , say, then the difference between the before and after weight measurements of the ablating sample will give a value for the total mass of gas evolved ($\dot{m}_g$) and lost as a result of the test. From a calibration measurement using a non-ablating calorimeter (with provision for the measurement of the surface temperature by optical pyrometry, say,) the total heat flux to the sample may be determined for known arc-jet or torch conditions. Thus, on a unit time basis, the Q* so measured can be related to the energy fluxes existing in Zone II of the aft-closure by,

$$Q^* = \frac{q_c + q_r + q_p}{\dot{m}_g} \tag{41}$$

where, for char forming elastomeric insulating materials, the blowing effect (which decreases the net heat transfer to the wall) has been considered small relative to the sum of the fluxes given in the numerator. Blowing effects will probably be minimized, considering the secondary flows and particle effects, which would tend to counteract any boundary layer thickening caused by mass transfer. Nothing is now known concerning the gas composition given off at elevated temperatures by typical elastomeric insulation materials, though techniques for obtaining this information have been developed (38) for measuring the gas composition given off by plastic ablators and should be equally applicable to elastomeric materials. It is more appropriate to evaluate the importance of this effect when this information becomes available. The linear regression rate, r, is related to $\dot{m}_g$ as follows:

$$r = \frac{\dot{m}_{total}}{\rho_{in}} = \frac{\dot{m}_g + \dot{m}_c}{\rho_{in}} \tag{42}$$

where $\dot{m}_c$ is the mass of porous char formed per unit surface area and per unit time. Since the virgin material is homogeneous, then that portion of it which is transformed to the gas phase is proportional throughout the insulation material to that which forms the porous char. Also, since the char layer is assumed to be swept away as soon as it is formed, the following proportion,

$$\dot{m}_c = \frac{\rho_c}{\rho_{in}} (\dot{m}_g + \dot{m}_c) \tag{43}$$

may be used to eliminate $\dot{m}_c$ from Eq. (42) and thus obtain,

$$r = \frac{\dot{m}_g}{\rho_{in} - \rho_c} \tag{44}$$

where ρ_c is the density of the porous char ($\sim \rho_1$ in Grosh nomenclature). Eqs. (27), (28), (38), (41), and (44) can be combined to yield

$$r = \frac{[\sigma\epsilon(T_o^4 - T_w^4) + (h_c + \alpha_t \dot{m}_p c)(T_o - T_w)]}{Q^*(\rho_{in} - \rho_c)} \tag{45}$$

Using an estimate or measurement of T_w (see reference 39), and knowing Q^* as a function of $q_{total} = q_c + q_r + q_p$) for the particular insulation material of interest, then r may be calculated for each wall position in Zone II. Of course, h_c will depend on the static pressure gradient or U's employed as input to the Culick and Hill analysis. Methods such as cold or hot flow modeling need to be developed which will enable the prediction of reasonable estimates of this information as well as the ($\alpha_t \dot{m}_p$) at each position in Zone II as a function of time.

INPUT INFORMATION

In order to successfully apply the preceding considerations to the determination of the heat transfer rates and the insulation material removal rates in an aft closure, the following conditions and properties must be known (or estimated):

a. General flow, gas and particle properties:

(1) Rocket aft closure, and grain port nozzle geometry, and the change of grain port geometry with time.

(2) Grain port velocity (or C*).

(3) Propellant gas properties (thermodynamic and transport) including chemical state and initial particle mass fraction (neglecting the influence of the particles on the gas transport properties).

(4) Chamber pressure as a function of time including the total firing time, t_e.

(5) Chamber temperature (flame or stagnation temperature).

(6) Fluid velocities at edge of boundary layer (note that for $N_{Pr} \sim 1$ fluids, the momentum and thermal boundary layer thicknesses may be taken to be identical) at all times and positions.

(7) Inside wall (gas-char or gas-reaction zone interface) temperature as a function of axial position (note that in this analysis, a constant wall temperature has been assumed for each zone).

(8) The optical properties (i.e., complex refractive index) of the metal (oxide) particles at the chamber and aft-closure temperatures of interest as well as the number density of particles and particle size distribution appropriate for the given flow situation.

(9) Particle impingement rates ($\dot{m}_p$) at various locations and times in the aft-closure for given conditions 1 through 7.

(10) The energy accommodation (α_t) of the particles upon collision with the insulation wall for given conditions 1 through 7.

(11) A measure of the mechanical erosiveness of particles on both virgin insulation materials and their char layers.

b. Insulation material properties:

(1) The thermal conductivity, mass density and specific heat for the virgin material at a temperature between the ambient and mean reaction zone temperature.

(2) The thermal conductivity, mass density and specific heat of the porous char at a temperature between the mean reaction zone temperature and T_w (or the porosity of the char and the corresponding properties of the solid matrix material which makes up the char).

(3) The overall heat of pyrolysis and phase change (L_1) and the mean reaction zone temperature (T_1) and their possible dependence on the surface temperature.

(4) The composition, k, C_p and mass density of the gas mixture which transpires through the porous char layer at a temperature between the mean reaction zone temperature and the surface temperature (T_w) at the chamber pressure.

(5) Q* values for the ablative insulation material measured under specially designated experimental conditions (as a function of total incident heat flux and chamber pressure)

In regards to the present status of knowledge concerning each of the needed conditions and properties listed under a and b, the following information is not currently available and must at best, be crudely estimated (in some cases by techniques suggested in the previous sections): a-6 through a-11 with the possible exception of a-7 (39) and a-8 (28); and for elastomeric insulation materials, b-2 through b-5. A resonable analytical a priori determination of heat transfer in an aft closure requires knowledge of these properties.

OVERALL CALCULATION PROCEDURE

The analyses indicated above are integrated into a logical sequence of calculations to give the final insulation profile. The thickness of insulation that is either charred or removed in the recirculation zone, Δ_I, can be calculated as a function of time. Either by modeling the flow or by approximations based on theory (1), the location of the stagnation point can be prescribed as a function of time. Thus the length of time during which a particular point on the wall is in the secondary flow zone is known, and also the amount of material charred or removed during that time. After the stagnation point passes a point, it is assumed that the char is essentially removed and then the "fast" ablation continues. Using the Q* concept, one can write

$$\dot{r}(t) = \frac{q_p(t) + q_c(t) + q_r}{Q^*(\rho_{in} - \rho_c)} \tag{46}$$

If the values of $q_p(t)$ and $q_c(t)$ can be determined, $\dot{r}(t)$ can be determined and during fast ablation, the material removed is then

$$\Delta_{II} = \int_{t_s}^{t_e} \dot{r}(t)\, dt \tag{47}$$

To complete the determination of the amount of material removed, experimental data is needed as to the amount of mechanical erosion to be expected. Finally allowance must be made for the thermal penetration into the insulation at the end of the firing. This can be approximated from a steady state solution of the semi-infinite, one-dimensional conduction equation assuming a constant surface regression rate and a maximum allowable back wall temperature, T_{max}. The result of this is (see Baer and Ambrosio (40) Eqs. (30) and (31))

$$\Delta_p = -\frac{\kappa}{\dot{r}} \ln\left[\frac{T_{max} - T_i}{T_w - T_i}\right] \tag{48}$$

where $\dot{r}$ is the regression rate at burnout. The final insulation thickness required at a point is then

$$\Delta = \Delta_I + \Delta_{II} + \Delta_e + \Delta_p \tag{49}$$

where Δ_e denotes the total material removed due to mechanical erosion. For convenience of ordering the calculations the insulation wall positions at which material removal and thermal penetration are calculated are located along a line on the wall formed by the intersection of a plane through the axis and the wall. Circumferential variations can be included by rotating this plane and completing another set of calculations. The complete calculation outlined herein is dependent on the ability to describe the various phenomena discussed as functions of time and position. Figure 10 shows in schematic form the calculation procedure.

CONCLUSIONS

Although the prediction of insulation requirements in the aft-closure of a metallized solid propellant motor is of considerable importance, it is impossible to develop a usable, inclusive analysis of the problem because of the lack of information concerning many of the phenomena. In this report a calculation technique is developed which is a simplification of the total problem. For instance, effects such as the influence of boundary layer reactions upon heat transfer, the reduction of the convective flux due to blowing, and wall roughness have not been considered. However, an attempt has been made to include those effects that are felt to be of prime significance. A method of handling each of these effects is suggested and then the missing, necessary information is identified. In conclusion, the method described herein should provide relatively accurate predictions of aft-closure insulation requirements when the following data becomes available:

(1) Pressure and velocity at the edge of the boundary layer at any time and position in the aft closure.

(2) Particle impingement rates at various locations and times in the aft closure.

(3) Methods for estimating the accommodation of the energy of the particles upon collision.

(4) Estimation of the mechanical erosiveness of particles on both virgin insulation materials and their char layers.

(5) The complex refractive index of the metal oxides at elevated temperatures.

(6) The physical properties of the virgin ablators and their char layers.

(7) Q* values for ablators measured under specially designated experimental conditions.

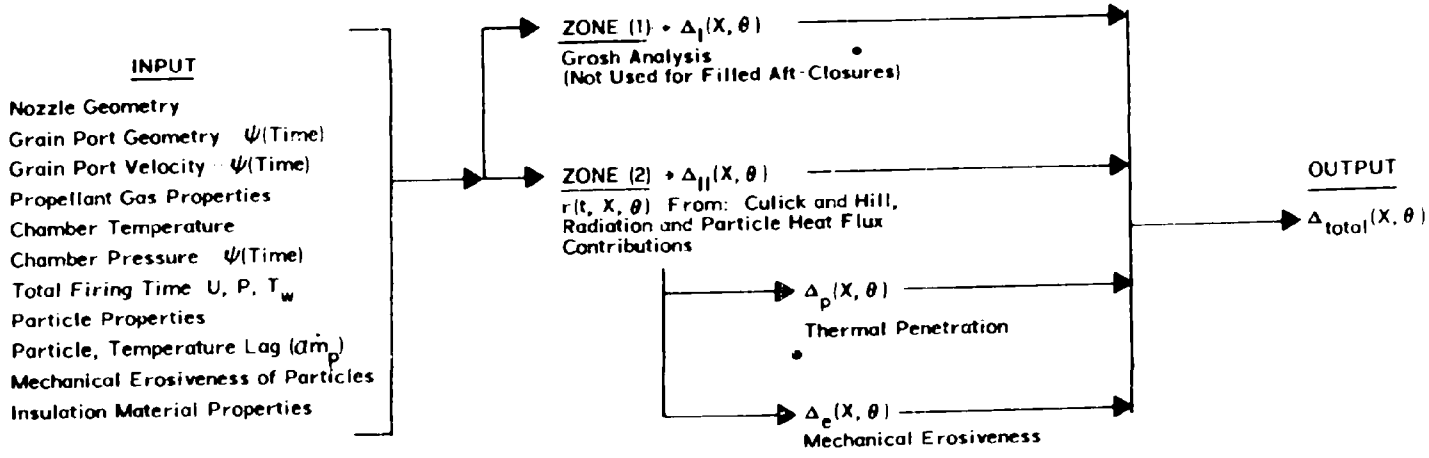

Fig. 10 Schematic Calculation Procedure for Determining Insulation Thicknesses.

NOMENCLATURE

A	local cross-sectional area of flow
A_*	cross-sectional flow area at nozzle throat
C_f	local skin-friction coefficient, $C_f \equiv \frac{2\tau_w}{\rho U^2}$
C_p	specific heat of the gas at constant pressure
C^*	characteristic velocity (see reference 11)
c	heat capacity of particles
D_*	diameter at the nozzle throat
g	gravitational acceleration (32.17 ft/sec^2)
g_c	gravitational conversion factor ($32.17 \frac{lb}{lb_f} \frac{ft}{sec^2}$)
H	boundary-layer shape parameter (see Reference 17)
h_c	local convective heat-transfer coefficient
J	mechanical equivalent of heat ($778.2 \frac{ft\ lb_f}{Btu}$)
L	Truckenbrodt's shape factor (see Reference 17)
ℓ	optical cross-section of cloud
M	Mach number at the edge of the boundary layer
M_g	molecular weight of propellant gas mixture flowing through aft closure
$\dot{m}_g$	rate of gas evolution of ablating insulation material per unit surface area
$\dot{m}_p$	rate of particle impingement per unit area
k	proportionality constant
N	particle number density
N_{Pr}	Prandtl number of the propellant gas mixture
P_c	chamber pressure
Q_{ext}	extinction coefficient

NOMENCLATURE (Continued)

Q^*	effective heat of ablation for insulating material (see Eq.41)
q_c	convective heat flux per unit area
q_r	radiative heat flux per unit area
q_p	energy exchange per unit area as a result of particle impingements
r	linear regression rate of insulating materials
r'	recovery factor, taken to be $N_{Pr}^{1/3}$ for turbulent flow
r_c	radius of wall curvature at the nozzle throat
R	local radial distance from the rocket motor centerline
R_p	radius of particles
R_o	Gas Law constant = 1.987 Btu/lb mole °R
T	static gas temperature at the edge of the boundary layer
T_i	initial temperature of the insulation
T_o	stagnation temperature of gas free stream
T_p	temperature of particles
T_{aw}	adiabatic wall temperature
T_w	temperature of wall
t_e	total firing time
t_s	time at which flow stagnation point moves past a given station after ignition
U	local edge-of-boundary-layer velocity
v_{P_i}	volume of typical particle
X	cloud path length or axial position in nozzle measured from the start of the aft closure
x	distance along the surface in the direction of flow

Greek Symbols

α_t impinged particle's thermal-accommodation coefficient

β Falkner-Skan pressure gradient parameter (see reference 17, p. 132)

γ ratio of specific heat at constant pressure to that at constant volume (frozen)

Φ ratio of the mass flow rate of particles to the mass flow rate of the gas

ϵ effective emissivity (see Eq. 39)

σ Stefan-Boltzmann constant, Eq. (38)

σ $\left(\frac{\rho_{am}}{\rho}\right)^{0.8}\left(\frac{\mu_{am}}{\mu_o}\right)^{0.2}$ in Eq. (12)

σ_{abs} absorption cross-section

σ_{eff} effective cross-section

σ_{sc} scattering cross-section

ρ_{in} density of insulating material

κ thermal diffusivity of insulation

θ boundary-layer momentum thickness, or angular position under the propellant grain star configuration (see Figure 10)

μ viscosity: μ_*, viscosity at the reference temperature, T_* in Sutherland's law (see Eq. 16)

ν kinematic viscosity, $\nu = \mu/\rho$

ρ local mass density of the gas at the edge of the boundary layer

ρ_s density of a particle

τ_w shear force at the wall

Subscripts

am	arithmetic mean (wall-free stream)
aw	adiabatic wall
i	corresponding quantities in the related incompressible flow
in	virgin insulation material
0	stagnation conditions
TR	conditions at the point of transition from laminar to turbulent flow
∞	conditions at some reference point; e.g., in the free stream, at the propellant grain port, or at the transition point
*	conditions at the throat
total	length from start of aft closure to end of exit cone

REFERENCES

1. Pai, Shih-I, Fluid Dynamics of Jets, Van Nostrand Co., Inc., New York, 1954, p 139.

2. Price, F. C., et al. "Detail Design Optimization of Solid Propellant Rocket Motor Aft-Closure Nozzle Combinations (U)." Third Quarterly Progress Report (Confidential), Publication C-1635. Newport Beach, California: Aeronutronic Division, Ford Motor Company (April 5, 1962) (ASTIA AD 328912).

3. Grosh, R. J., "Transient Temperature in a Semi-Infinite, Porous Solid with Phase Change and Transpiration Effects." WADD TR 60-105. Lafayette, Indiana: Midwest Science Corporation (January 1960).

4. Scala, Sinclaire M. and Gilbert, Leon M. "Thermal Degradation of a Char-Forming Plastic During Hypersonic Flight." ARS Journal, Vol. 32 (June, 1962), pp. 917-924.

5. Carslaw, H. S., and Jaeger, J. C., Conduction of Heat in Solids. Second Edition. Oxford at the Claredon Press (1959), pp. 283-287.

6. Perry, J. H. (Editor), Chemical Engineer's Handbook. Third Edition. New York: McGraw-Hill Book Company (1950).

REFERENCES (Continued)

7. Hazelrigg, W. K. (Solid Rocket Plant, Aerojet-General Corp., Sacramento, California) Personal Communication (February 1962)(see Reference 41).

8. Solanski, A. H., et al. Dynamics of Separating Bodies Vol I "Theoretical Analysis," AFOSR TR-109, Holloman AFB, New Mexico; Directorate of Research Analysis, March 1961, p. 32 (ASTIA AD271998).

9. Nickelson, H. M. and Fields, J. P. "Some Experimental Techniques to Investigate the Mechanism of Flame Stabilization in the Wake of Bluff Bodies," Third Symposium on Combustion, Flame, and Explosion Phenomena Williams and Wilkins Co., 1949.

10. Bartz, D. R., "A Simple Equation for Rapid Estimation of Rocket Nozzle Convective Heat-Transfer Coefficients," Jet Propulsion, Volume 27, No. 1 (January 1957) pp. 49-51.

11. Welsh, W. E., Jr., and Witte, A. B., "A Comparison of Analytical and Experimental Local Heat Fluxes in Liquid-Propellant Rocket Thrust Chambers," Tech, Report No. 32-43, Jet Propulsion, Pasadena, California. (See also ASME Paper No. 61-AV-59.)

12. Eckert, E. R. G., "Survey of Boundary Layer Heat Transfer at High Velocities and High Temperatures." WADC TR 59-624 (April 1960).

13. Krieve, Walter F. and Mason, David M., "Heat Transfer in Reacting Systems: Heat Transfer to Nitrogen Dioxide Gas under Turbulent Pipe Flow Conditions, A.I.Ch.E. Journal, Vol. 7 (June 1961) pp. 277-281. See also: JPL Progress Report 20-366.

14. Richardson, J. L., et al., "Heat Transfer in Reacting Systems -- Heat Transfer to N_2O_4 Gas Flowing Normal to a Heated Cylinder," Chemical Engineering Science, Vol. 13 (February 1961) pp. 130-142.

15. Culick, F.C.C., and Hill, J.A.F., "A Turbulent Analog of the Stewartson-Illingworth Transformation," Journal of the Aeronautical Sciences, Vol. 25, No. 4 (April 1958), pp. 259-262.

16. Truckenbrodt, E., "A Method of Quadrature for Calculation of the Laminar and Turbulent Boundary Layer in Case of Plane and Rotationally Symmetrical Flow," NACA TM 1379 (1955).

17. Schlichting, Hermann, Boundary Layer Theory, 4th Ed., McGraw-Hill (1960) p. 574. Ibid., p. 190.

18. Rotta, J. "Näherungsverfahren zur Berechnung Turbulenter Grenzschichten unter Benutzung des Energiesatzes." Mitteilungen Nr. 8. Göttingen: Max-Planck - Institut für Strömungsforschung (1953). See also, Rotta, J. "On the Theory of the Turbulent Boundary Layer." NACA TM 1344 (1953); and Rotta, J. "Schubspannungsverteilung und Energiedissipation bei Turbulenten Grenzschichten." Ingenieur-Archiv, Vol. 20 (1952), pp. 195-207.

19. Michel, R., "Etude de la Transition sur les Profile D'Aile; Establishment d'un Critere le Determination du Point de Transition et Calcul de la Trainee de Profile en Incompressible," ONERA Report 1/1578A (1951). See also, ONERA (France) Publication No. 58 (1952).

20. Smith, A.M.O., "Transition, Pressure Gradient and Stability Theory," 9th International Congress of Applied Mechanics, Vol. 4, (1957) Brussels, Belgium: University of Brussels, pp. 234-244. See also, Smith, A.M.O. and Gamberoni, Nathalie "Transition, Pressure Gradient and Stability Theory." Report No. ES 26388. El Segundo, California: Douglas Aircraft Co., Inc. (Aug. 31, 1956).

21. Eckert, E., "Survey on Heat Transfer at High Speeds, " WADC Technical Report 54-70, Wright Air Development Center (April 1954) p. 37-39.

22. Rubesin, Morris W. "A Modified Reynolds Analogy for the Compressible Turbulent Boundary Layer on a Flat Plate." NACA TN 2917 (1953).

23. Ziebland, H. "Heat Transfer Problems in Rocket Motors," J. British Interplanetary Society, Vol. 14 (1955) pp. 249-264 (see page 257 in particular).

24. Bartz, Donald B. "An Approximate Solution of Compressible Turbulent Boundary Layer Development and Convective Heat Transfer in Convergent-Divergent Nozzles." External Publication No. 243. Pasadena, California: Jet Propulsion Laboratory (1955). See also, ASME Transactions (Nov., 1955), pp. 1235-45.

25. Johnson, H. A., and Rubesin, M. W., Trans, ASME, Vol. 71, pp. 447-456 (1949).

26. Ungar, E. W., "Particle Impacts on the Melt Layer of an Ablating Body," ARS Journal, Vol. 30 (September 1960) pp. 799-805.

27. Farbar, L., and Morley, M. J., "Heat Transfer to Flowing Gas-Solids Mixtures in a Circular Tube," Ind. and Eng. Chemistry, Vol. 49, No. 7 (July 1957) p. 1143.

28. Carlson, D. J., "Experimental Determination of Thermal Lag in Gas-Particle Nozzle Flows." Accepted for publication in ARS Journal (1962).

29. Stull, V. Robert, and Plass, Gilbert N., Emissivity of Dispersed Carbon Particles," Journal of Optical Society of America, Vol. 50, No. 2, pp. 121-129 (February 1960).

30. Van De Hulst, H. C., Light Scattering by Small Particles, Wiley, New York, 1957, p. 129.

31. Kliegal, J. R., and Nickerson, G. R., "Flow of Gas-Particle Mixtures in Axially Symmetric Nozzles," ARS Preprint 1713-61 (1961).

32. Spalding, D. B., "The Theory of Melting Ablation, with Vaporisation, Gas-Phase Chemical Reaction, Surface Pyrolysis, and Transient Effects," Journal of the Aeronautical Quarterly, London (August 1961), pp 237-74.

33. Adams, Mac C., "Recent Advances in Ablation," ARS Journal, Vol. 29 (September 1959) pp. 625-632.

34. Barriault, R. J. and Yos, J., "Analysis of the Ablation of Plastic Heat Shields that Form a Charred Surface Layer," ARS Journal, Vol. 30 (September 1960) pp. 823-829.

35. Scala, S. M., "A Study of Hypersonic Ablation," Space Sciences Laboratory, General Electric, Missile and Space Vehicle Department, Technical Information Series No. R59SD438 (September 1959) Presented at Tenth International Astronautical Federation Congress, 29 August - 5 September, 1959, London, England.

36. Munson, T. R., and Spindler, R. J., "Transient Thermal Behaviour of Decomposing Materials," Research and Advanced Development Division, Avco Corporation, Wilmington, Massachusetts (1961).

37. Lafazan, S. and Siegel, B., "Ablative Thrust Chambers for Space Application," Paper No. 5, Presented at American Institute of Chemical Engineers, 46th National Meeting, Los Angeles, Calif. (February 5, 1962). Los Angeles, California: Aerospace Corp.

38. Schwartz, H. S. (Editor), "Conference on Behavior of Plastics in Advanced Flight Vehicle Environments." WADD Technical Report 60-101, ASTIA AD 247100 (September 1960).

39. Brookley, C. E , "Measurements of Heat Flux to the Internal Insulation of a Rocket Motor." Allegany Ballistics Laboratory Research Progress Report A2-53. Cumberland, Maryland: Hercules Powder Company (November 2, 1961).

40. Baer, D., and Ambrosio, A., "Heat Conduction in a Semi-Infinite Slab with Sublimation at the Surface." STL report TR-59-0000-00610. Los Angeles, California: Space Technology Laboratories, Incorporated (February 24, 1959).

41. Epstein, G., "Status Report on Internal Insulation." Aerojet Report RD-R60-86. Azusa, California: Aerojet-General Corporation (September 26, 1960). Also; Hartz, Walter A., Personal Communication, General Tire and Rubber Co., Akron, Ohio (May, 1962).

42. Bradshaw, W. G., and Matthews, C. O., "Properties of Refractory Materials: Collected Data and References." LMSD-2466. Sunnyvale, California: Missile Systems Division, Lockheed Aircraft Corporation (June 24, 1958), ASTIA AD 205452, Page 73.

43. Smith, J. M., Introduction to Chemical Engineering Thermodynamics. New York: McGraw-Hill Book Company (1949), p. 94.

44. Jones, Warren C. (Materials Central, Wright-Patterson AFB, Ohio). Personal Communication (June 22, 1962).

45. R. Sehgal, "An Experimental Investigation of a Gas-Particle System." Technical Report No. 32-238. Pasadena, California: Jet Propulsion Laboratory (March 16, 1962).